



# Nano-structured self-assembled $\text{LaCrO}_3$ thin film deposited by RF-magnetron sputtering on a stainless steel interconnect material

Christopher Johnson<sup>a</sup>, Randall Gemmen<sup>a</sup>, Nina Orlovskaya<sup>b,\*</sup>

<sup>a</sup>National Energy Technology Laboratory, Department of Energy, 3610 Collins Ferry Road, Morgantown, WV 26507, USA

<sup>b</sup>Department of Materials Science and Engineering, Drexel University, 3141 Chestnut Street, Philadelphia, PA 19104, USA

Received 15 July 2003

## Abstract

The deposition of an amorphous La–Cr–O thin film on a stainless steel was done by radio frequency magnetron sputtering to obtain a protective coating on the metallic interconnect for solid oxide fuel cells. The deposited film was amorphous, but underwent two-phase transformations to the perovskite structure as a result of annealing at 700 °C for 1 h. The first transformation was from amorphous to the monoclinic  $\text{LaCrO}_4$  monazite type compound. The second transformation was from  $\text{LaCrO}_4$  to orthorhombic  $\text{LaCrO}_3$  perovskite. As a result of the phase transformation nano-structured self-assembled dendritic structure was formed with the desired perovskite phase. The structural characterization of the film was done by X-ray diffraction, phase shift microscopy, scanning electron microscopy with energy dispersive X-ray analysis, and micro-Raman spectroscopy.

© 2003 Elsevier Ltd. All rights reserved.

**Keywords:** Perovskite; Lanthanum chromite; Amorphous to crystalline phase transition; Self-assembled nano-structure; Micro-Raman spectroscopy; Thin film; Solid oxide fuel cells

## 1. Introduction

Energy conversion using solid oxide fuel cells (SOFCs) is a highly efficient and an environmentally friendly technology [1]. Unlike lower temperature fuel cells, SOFCs can use both hydrogen and carbon monoxide as fuels, thus any traditional synthesis gas source is a potential fuel for SOFC applications. At the current operating temperatures (600–800 °C) it is also possible to reform hydrocarbon fuels on the anode side of the fuel cell. The direct electro-conversion of fuel into electrical energy with a high efficiency is particularly attractive.

Since the early 1960s, the development of SOFC technology has been primarily directed toward manufacturing of electrical generation plants and the R&D of SOFCs was mostly on > 100 kW systems with robust design and high temperature operation (1000 °C) for high output power. The need for high temperature operation originated

from the necessity to increase the ionic conduction through the electrolyte for efficient SOFC operation. Such high temperatures strongly limited the choice of materials because of significant thermal degradation. Overcoming some of the materials degradation issues has led to the development of intermediate temperature SOFCs (IT-SOFCs) that are categorized as operating at 600–800 °C, although 800 °C is more typical. The lower temperature of operation makes less expensive materials more viable candidates and also opens up opportunities for new applications. For example, one very promising application of IT-SOFCs is to produce 1–25 kW units for automotive applications. Another recent SOFC development is miniaturized units of 100 mW–1 W for portable electronics devices. Commercialization of these applications will require even lower operating temperatures and additional materials improvements.

A single SOFC consists of an air electrode (cathode), an electrolyte, and fuel electrode (anode). The typical materials set for the IT-SOFCs are perovskite cathodes such as  $\text{La}_x\text{Sr}_{1-x}\text{MnO}_3$ , Ni– $\text{YZrO}_2$  cermet anodes, and  $\text{Y}_2\text{O}_3$

\* Corresponding author. Tel.: +1-215-895-1541; fax: +1-215-895-6760.  
E-mail address: [orlovsk@drexel.edu](mailto:orlovsk@drexel.edu) (N. Orlovskaya).

stabilized  $\text{ZrO}_2$  electrolyte. The cells are separated by interconnects which serve to electrically connect the cells, separate fuel and oxidant flows, and to distribute gases in the proper directions and provide structural integrity [3]. When SOFCs were operated at  $1000^\circ\text{C}$ ,  $\text{LaCrO}_3$  based perovskites were the only choice available as an interconnect material for such high temperature SOFC applications [2]. As research moved to the IT-SOFCs and even nano-structured low temperature (LT) SOFCs, another prospective interconnect material emerged [4,5]. The Cr containing stainless steel (SS) is seriously being considered to substitute for the brittle and unreliable  $\text{LaCrO}_3$  perovskite as an interconnect material for IT and LT applications.

The limiting factor for use of the metallic interconnect in SOFCs is a low corrosion resistance and a formation of pure conducting oxide layers on the cathode side when interconnect is exposed to the oxidative environment [6]. The metallic materials may require an additional coating in order to achieve the long lifetime required for commercial systems ( $>40,000$  h). To protect metallic interconnect against oxidation at least two different strategies have been used. One of them is the addition of thin layers of surface dopants [7,8] such as Y, La, and Ce that can change the growth mechanism of the oxide scale on the Cr containing alloy's surface; and a second one is the coating of the interconnect with a conducting oxide layer such as an electrically conductive perovskite to suppress oxidation [9,10].

Here we report a feasibility study on  $\text{LaCrO}_3$  thin film deposition on SS 446 substrates and a characterization of the film's structure. The  $\text{LaCrO}_3$  perovskite thin film deposited by RF-magnetron sputtering on the Cr containing SS as a protective coating against interconnect oxidation in the aggressive SOFC environment is under consideration.

## 2. Experimental

Thin films were deposited by RF-magnetron sputtering on the Cr containing SS substrates. High chromium ferritic Fe–25Cr steel coupons (SS 446) with the chemical composition Fe (74 wt%), Cr (23 wt%), Mn (1.5 wt%), Ni (0.3 wt%), Si (1.0 wt%), C (0.2 wt%) were used as a substrate material. SS substrates ( $10 \times 10 \times 5 \text{ mm}^3$ ) were polished with a diamond spray to a mirror surface. The schematics of the sputter down system set up are presented in Fig. 1A. The magnetron sputtering was performed at Thin Films, Inc. The substrates were coated in the RF-sputtering mode under  $8 \times 10^{-3}$  Torr  $\text{Ar}^+$ . The substrate temperature was  $25^\circ\text{C}$  at the beginning of deposition. The target to substrate distance was 5 mm. After pre-sputtering the target for 30 min, the substrates were moved into position under the target and then remained stationary. The total time of sputter deposition, at 500 W power, was 5 h. Highly porous (40%) light green color  $\text{LaCrO}_3$  perovskite was used as a target material (Fig. 1B). Energy Dispersive Spectroscopy (EDS) analysis of the target  $\text{LaCrO}_3$  show a slight excess of

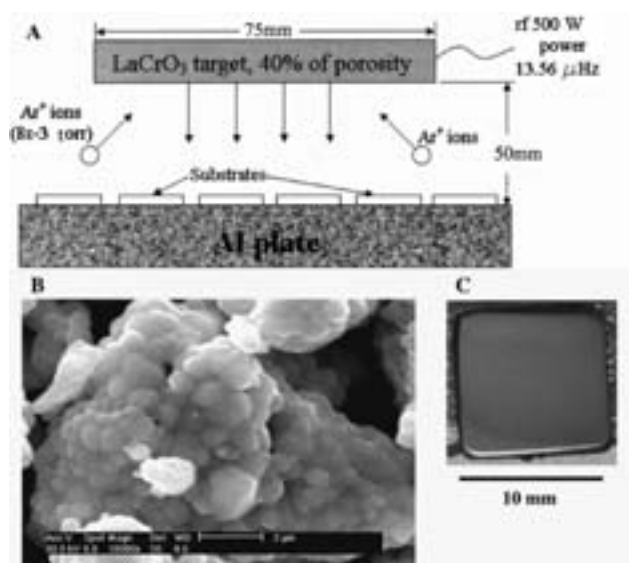


Fig. 1. (A) A schematic presentation of RF-magnetron sputtering deposition process. (B) A micrograph of the  $\text{LaCrO}_3$  perovskite target microstructure. (C) A photograph of an amorphous La–Cr–O thin film after deposition.

Cr with 49.11/50.89 at.% La/Cr ratio. The light green color thin film was deposited (Fig. 1C). The EDS of an as-deposited film composition gave 56.54/43.46 at.% La/Cr ratio. After sputtering, the SS sample with deposited film was annealed at 300 and  $500^\circ\text{C}$  for 15 min, and finally at  $700^\circ\text{C}$  for 1 h using a controlled heating rate of  $30^\circ\text{C}/\text{min}$ . After dwelling at  $700^\circ\text{C}$  for 1 h the sample was taken out of the furnace and cooled in air. After annealing X-ray diffraction (XRD) pattern was acquired from the  $\text{LaCrO}_3$  deposited SS sample.

Environmental scanning electron microscopy (SEM), interferometric surface profiler with phase shift technology and optical microscopy were used for characterization of the surface morphology and microstructure of the thin films. A Siemens diffractometer was used to determine the crystal structure of the thin films. A micro-Raman spectrometer Renishaw 1000 was used to study the vibrational spectra of the thin film. The excitation light was a 514.5 nm line of  $\text{Ar}^+$  Ion laser. The incident and scattered beams were focused using an Olympus microscope with  $50\times$  objective and a laser spot as low as  $4\text{--}5 \mu\text{m}$ . All measurements were performed at room temperature. The Raman bands were deconvoluted using Grams software.

## 3. Results and discussion

Film thickness measured with an interferometric surface profiler with phase shift technology was  $0.2 \mu\text{m}$  (Fig. 2A). The 'as-deposited' film was very smooth and had high quality of the surface (Fig. 2B). The amorphous nature of the as-deposited film was confirmed by XRD [11]. There was a very small amount of oxygen ( $\sim 20$  at.%) present in as-deposited film.

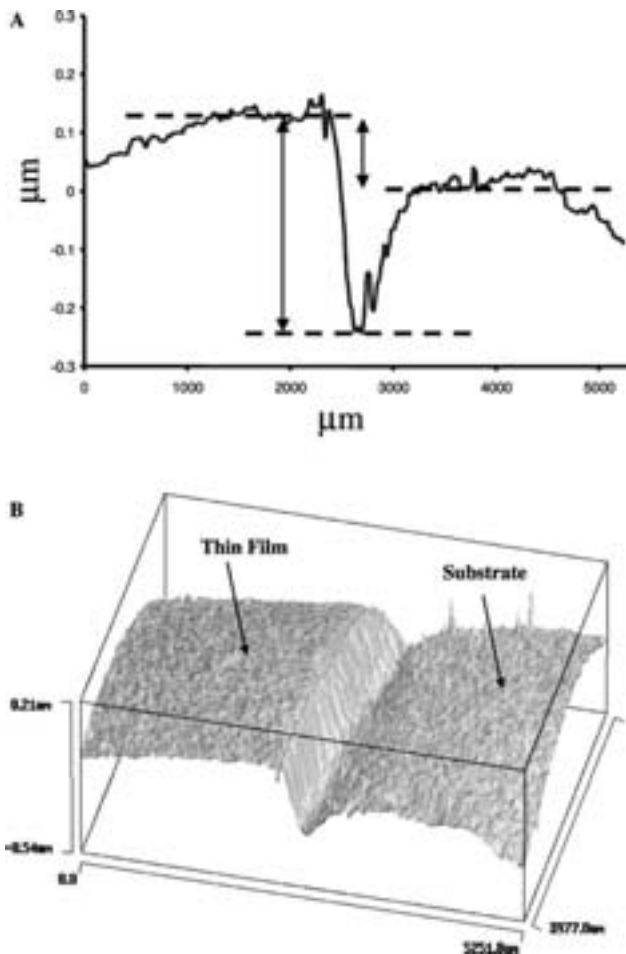


Fig. 2. Thickness (A) and surface morphology (B) of as-deposited La–Cr–O film were measured by interferometric surface profiler, phase shift technology.

After annealing at 700 °C for 1 h, the perovskite structure was developed and several distinctive structural features are present (Fig. 3). Large grain regions could be clearly seen in the micrographs (Fig. 3A), most of them with cracks at the edges that expose the SS 446 surface to the environment. Additionally, a fine dendrite structure grew during annealing and such structure was especially well pronounced in the large grains with the size of individual dendrites reaching 300 nm. The film structure inside the grains consists of small dendrites that tend to be organized in a self-assembled structure on the surface (Fig. 3B). All dendrites have a roundish morphology. The oxygen content in the annealed film was much higher, as a result of annealing being done in air. While it was expected that the perovskite structure would be formed at or above 780 °C [12], we found the  $\text{LaCrO}_3$  perovskite after annealing at as low as 700 °C for 1 h. One possible explanation for the lower temperature formation may be that the very same sample was annealed first at 300 °C, and then at 500 °C for 15 min, before annealing at 700 °C, therefore, such LT short term annealing facilitates the perovskite phase formation.

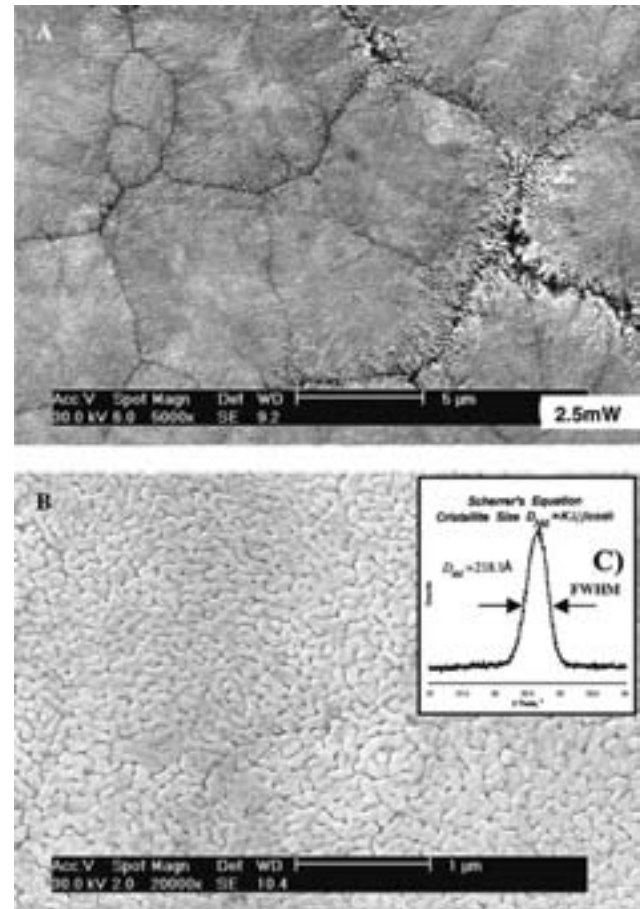


Fig. 3. Micrographs of the  $\text{LaCrO}_3$  perovskite structure formed after annealing of amorphous film at 700 °C for 1 h. (A) A dendritic structure of  $\text{LaCrO}_3$  perovskite. (B) A self-assembled structure of  $\text{LaCrO}_3$  crystallites inside grains. (C) Inset: full width at half maximum of {111} peak and calculated crystallite size of the  $\text{LaCrO}_3$  thin film.

The cracks formation at the boundaries of large grains was a result of shrinkage during crystallization of the amorphous film. Another important factor that contributed to the crack formation and has to be considered here is the mismatch in coefficient of thermal expansions (CTEs) of the thin film and the SS substrate material. The CTE of SS is  $10 \times 10^{-6} \text{ K}^{-1}$  and the CTE of  $\text{LaCrO}_3$  is  $9 \times 10^{-6} \text{ K}^{-1}$  [13,14]. This results in development of compressive residual stresses in the film during cooling after annealing. It is known that crystallization of the amorphous film occurs via nucleation and subsequent grain growth [15]. First, local ordering occurs without significant requirement of nucleation that leads to a locally ordered structure composed of medium-range and short-range ordered clusters. Such locally ordered structure is more stable than the amorphous phase, but it has no characteristics of a crystalline phase such as clearly visible peaks in XRD pattern or diffraction spots in the transmission electron diffraction pattern. Such local structural inhomogeneities in the amorphous state are one of the parameters that controls further heterogeneous nucleation and crystal growth process during amorphous–crystalline transition [16]. When local ordering dominates,

the transformation upon annealing leads to a structure composed of very small short- or medium-range ordered clusters, and the process does not require significant nucleation of critical nuclei. The earliest stage of crystallization is the hardest to observe, yet it usually dictates the rest of the growth process. There is always a ‘free-energy barrier’ to nucleation, because creating a new interface between different clusters costs free energy. And such costs are higher for small clusters or nuclei because they have a higher ratio of surface area to bulk volume, so small clusters have to reach a certain size to stand a chance of surviving [17]. After the formation of locally ordered structure, further heating initiates long-range ordering (crystallization) of the structure that is dominated by nucleation and grain growth and the formed precipitates are rather large. Both these processes reduce the free energy of the material, and, therefore, provide a thermodynamic driving force. The question that needs to be answered is whether crystallization starts at the film-substrate interface with crystals growing to the surface, or crystallization starts from the film surface.

It was reported recently that in the case of La–Cr–O compounds, the amorphous to the monoclinic monazite type  $\text{LaCrO}_4$  phase transition occurs at 495–530 °C. The reaction is exothermic [12]. In a separate set of experiments, the results of which will be presented elsewhere [18], we annealed separate samples of similar amorphous films at selected temperatures (300, 400, 500, 600, 700, 800, and 900 °C) for 1 h without any preliminary heat treatment. In these experiments, similar results were obtained as in Ref. [12] on La–Cr–O thin film, with no diffraction pattern observable on the as-deposited film, or after annealing at 300 or 400 °C for 1 h. At 500 °C some very small peaks, almost non-distinguishable from the background could be found. However, Raman spectroscopy revealed a significant increase in the intensity of the bands that belong to  $\text{LaCrO}_4$  structure for the thin film annealed at 500 °C for 1 h [11]. To find more definitive answers on the structure of La–Cr–O film annealed at 500 °C, transmission electron microscopy together with convergent-beam electron diffraction should be performed [19]. Films annealed at 600 and 700 °C showed a monoclinic structure of monazite type  $\text{LaCrO}_4$ , as confirmed by XRD and Raman spectroscopy. The reaction of the decomposition of  $\text{LaCrO}_4$  to  $\text{LaCrO}_3$  perovskite further occurs at 780–840 °C. The reaction  $\text{LaCrO}_4$  (monoclinic)  $\rightarrow$   $\text{LaCrO}_3$  (orthorhombic) +  $0.5\text{O}_2$  is endothermic and TG data showed a weight decrease that correspond to the oxygen removal from the lattice [12]. The  $\text{LaCrO}_4$  decomposition is considered to be composed of the four elementary reactions: (a) nucleation and growth of  $\text{LaCrO}_3$ ; (b) a phase-boundary reaction between  $\text{LaCrO}_4$  and  $\text{LaCrO}_3$ ; (c) diffusion of oxygen species through the  $\text{LaCrO}_3$  layer; and (d) an evolution of  $\text{O}_2$  gas. As one of the possible mechanisms of the oxygen evolution, the absorption of the oxygen species on the  $\text{LaCrO}_3$  surface prior to deoxygenation was also proposed. The molecular volume and theoretical density of  $\text{LaCrO}_4$  are  $82.30 \text{ \AA}^3 \text{ molecule}^{-1}$

and  $5.15 \text{ g/cm}^3$ , respectively, and for  $\text{LaCrO}_3$  these values are  $58.58 \text{ \AA}^3 \text{ molecule}^{-1}$  and  $6.77 \text{ g/cm}^3$ , respectively [20]. Therefore, the loss of oxygen in  $\text{LaCrO}_4$  leads to about 30% decrease of molecular volume, which corresponds to about 10% decrease in the grain diameter of  $\text{LaCrO}_3$ . It was reported [21] that  $\text{LaCrO}_4$  compound is reversible in a reduction–reoxidation treatment, and, while reduced to  $\text{Cr}^{3+}$  perovskite structure, could be restored by reoxidation in high oxygen partial pressure atmospheres. In our study, only the  $\text{LaCrO}_4$  phase was found as an intermediate product of the amorphous to perovskite structure phase transition, and no other mixed oxides compounds, such as  $\text{La}_2\text{CrO}_6$  or  $\text{La}_2(\text{CrO}_4)_3$  phases, were detected. The thin film annealed at 800 °C for 1 h showed  $\text{LaCrO}_3$  perovskite structure, however, in the thin film annealed at 900 °C both  $\text{LaCrO}_3$  perovskite and  $\text{LaCrO}_4$  monazite type structures were found. Thus, two transitions, one from amorphous to monoclinic  $\text{LaCrO}_4$  monazite type phase, and a second one from  $\text{LaCrO}_4$  to orthorhombic  $\text{LaCrO}_3$  perovskite phase, were detected during annealing of La–Cr–O thin films. The discussion on the detailed mechanisms of the amorphous to perovskite structure phase transitions will be presented in full detail elsewhere [18].

The structural changes occurring during the amorphous to crystalline transition have a clear tendency to generate self-organized network [22]. It was pointed out that in amorphous material there are non-random structural networks that go beyond just simple chemical ordering. It was also pointed out that such networks could self-organize. Such self-organization decreases the local degrees of freedom of the structure and some constraints in the film are removed [23]. The development of the self-organized model leads to an understanding of the necessity of two phase transitions and an intermediate phase that should be rigid but stress-free [22]. In case of the La–Cr–O thin film, it was demonstrated that an amorphous to perovskite structure transition occurs via two steps: a first step is an amorphous to monoclinic  $\text{LaCrO}_4$  monazite phase, as an intermediate phase transition, and a second step is when the  $\text{LaCrO}_4$  transforms to the  $\text{LaCrO}_3$  perovskite. The self-assembled structures of  $\text{LaCrO}_3$  perovskite phase was demonstrated as a result of all the different processes that occurred during heat-induced crystallization from the amorphous state (Fig. 3B).

The formation of perovskite structure after annealing at 700 °C for 1 h was confirmed by XRD [11]. The crystallite size is one of the important parameters of the perovskite structure, therefore it is important to calculate it. It is well known [24] that the peak width in the XRD pattern is related to the size of crystallites that compose the material. Besides the minuteness of the crystallite, non-uniform distortion of the crystallite is another factor that causes the broadening of peak width. Accordingly, the size of the average crystallite can be determined by measuring a peak width. The size of the crystallite is inversely proportional to the peak width. Scherrer’s equation  $D_{hkl} = k\lambda/\beta \cos \theta$ , where  $\lambda$  is the X-ray

wavelength for measurement ( $\text{\AA}$ ),  $\beta$  is the full width at half maximum (FWHM) due to crystallite size (rad),  $\theta$  is the Bragg angle of diffracted rays,  $k$  is a constant, was used for calculation of the crystallite size of  $\text{LaCrO}_3$  perovskite. The calculated size of the  $\text{LaCrO}_3$  crystallite was 22 nm. The  $\{112\}$  peak was used to calculate the crystallite size, which turned out to be much smaller than the average size of the small dendrites that make up the larger grains of the films. It means that each dendrite consists of 5–7 crystallites.

While X-ray analysis did not reveal any specific differences between  $\text{LaCrO}_3$  perovskite target material and  $\text{LaCrO}_3$  thin film annealed at  $700^\circ\text{C}$  for 1 h, the Raman spectra of the perovskite target and perovskite thin film were different (Fig. 4). The Raman spectrum of the porous target exhibits a strong dependence on the laser power/local heating of the surface (Fig. 4A). While bands at 154, 178, 260, 430, 590, 720, 1005, 1320, and  $1443\text{ cm}^{-1}$  wave numbers were observed at 2.5 and 6.25 mW laser power, with some of the bands actually consisting of several overlapping bands, both the intensity and FWHM of the bands were significantly changed when laser power was increased to 12.5 mW. All of the overlapping bands that were evident at lower laser power had almost disappeared

and what remained were single rather broad bands. As laser power increased even more to 25 mW, certain bands such as 154 and  $178\text{ cm}^{-1}$  disappeared entirely, and at lower wavenumbers bands were much lower in intensity and the width became very broad. It is clear that target material is very sensitive to local surface heating by the  $\text{Ar}^+$  Ion laser. The Raman spectrum of  $\text{LaCrO}_3$  perovskite, similar to the one that we collected from the target material, was published in Ref. [25].

Raman spectra collected from the perovskite thin film surfaces exhibit completely different features than those of the target material. The bands at 149, 172, 253, 427, 582, 695, and a small band at  $857\text{ cm}^{-1}$  are detected. Based on our previous results [11], we assigned a small  $857\text{ cm}^{-1}$  band to  $\text{Cr}^{5+}$  compound, and the rest of the band to  $\text{LaCrO}_3$  perovskite structure. Two bands at 149 and  $172\text{ cm}^{-1}$  can be assigned to La internal vibrations. Sometimes, three bands in this low wave number region can be collected, instead of two presented in Fig. 4B, all of them assigned to different modes of La vibrations. Two broad and strong modes at 582 and  $695\text{ cm}^{-1}$  could be tentatively assigned to O–Cr–O bending and stretching vibrations, while bands at the intermediate range of  $253\text{--}427\text{ cm}^{-1}$  can be assigned to octahedra rotational modes. The surface of  $\text{LaCrO}_3$  perovskite thin film is not sensitive to the laser overheating and the intensity of the spectra collected at different laser power increases as a laser power was increased from 2.5 to 25 mW. The differences in the Raman spectra collected from porous  $\text{LaCrO}_3$  target material and the  $\text{LaCrO}_3$  perovskite thin film requires further detailed investigation.

#### 4. Summary

Feasibility of deposition of La–Cr–O thin film by RF-magnetron sputtering was studied. A  $40\text{ nm/h}$  deposition rate was obtained and 5 h of deposition was required to grow a  $0.2\text{ }\mu\text{m}$  thin film. The as-deposited film was amorphous as confirmed by XRD. After annealing at  $700^\circ\text{C}$  for 1 h, the amorphous film transformed to  $\text{LaCrO}_3$  perovskite structure. Two steps occurred during such amorphous to perovskite structure transition: the first step is the amorphous to  $\text{LaCrO}_4$  monoclinic structure transition at  $495^\circ\text{C}$ , and the second step is the  $\text{LaCrO}_4$  to  $\text{LaCrO}_3$  orthorhombic structure transition at  $780^\circ\text{C}$ . However, in our case the temperature of the second transition was lowered to  $700^\circ\text{C}$  because of the preheating of the thin film sample at 300 and  $500^\circ\text{C}$  for 15 min. The nano-crystalline self-assembled dendritic structure of  $\text{LaCrO}_3$  perovskite thin film was demonstrated by SEM. The  $\text{LaCrO}_3$  orthorhombic perovskite was found to be a Raman active ceramic and the peculiarities of the Raman spectra of the  $\text{LaCrO}_3$  porous target material and the  $\text{LaCrO}_3$  thin film were discussed.

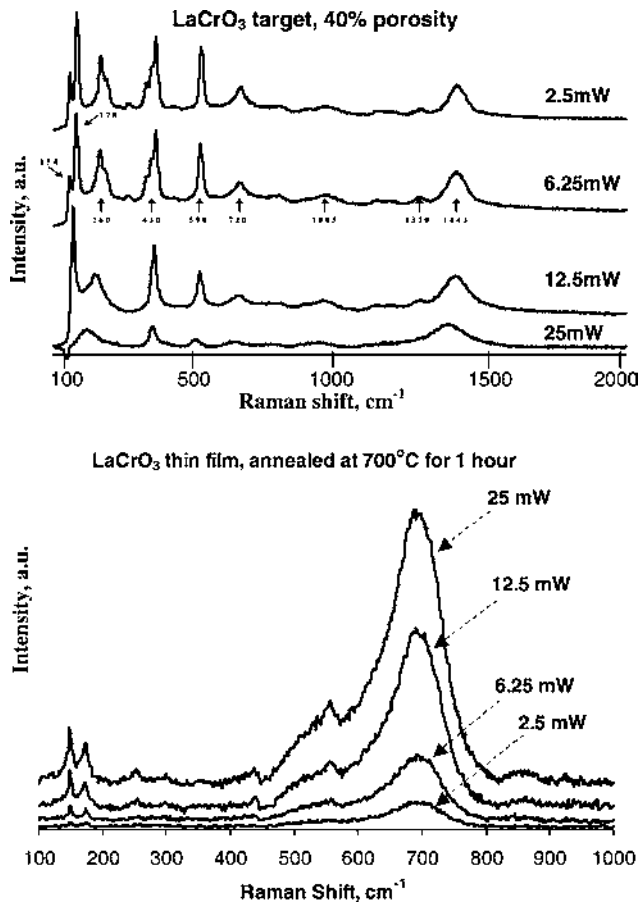


Fig. 4. Raman spectra of (A)  $\text{LaCrO}_3$  perovskite target and (B)  $\text{LaCrO}_3$  perovskite film as a function of laser power.

## Acknowledgements

The work at Drexel was supported by the National Energy Technology Laboratory, US Department of Energy under contract #239811.

## References

- [1] Singhal SC. Review: solid oxide fuel cells for stationary, mobile, and military applications. *Solid State Ionics* 2002;152–153:405–10.
- [2] Minh NQ, Takahashi T. Science and technology of ceramic fuel cells. Amsterdam: Elsevier; 1995. p. 1–366.
- [3] Zhu WZ, Deevi SC. Development of interconnect materials for solid oxide fuel cells. *Mater Sci Engng A* 2003;348:227–43.
- [4] Huang K, Hou PY, Goodenough J. Characterization of iron based alloy interconnects for reduced temperature solid oxide fuel cells. *Solid State Ionics* 2000;129(1–4):237–42.
- [5] Brylewski T, Przybylski K, Morgiel J. Microstructure of Fe–25Cr/(La, Ca)CrO<sub>3</sub> composite interconnector in solid oxide fuel cell operating conditions. *Mater Chem Phys* 2003;9801:1–4.
- [6] Kofstad P. In: Thorstensen B, editor. Proceedings of Second European Solid Oxide Fuel Cell Forum, 2, Oslo, Norway, May 6–10; 1999. p. 479.
- [7] Hou PY, Stringer J. The effect of reactive element additions on the selective oxidation, growth and adhesion of chromia scales. *Mater Sci Engng A* 1995;202(1–2):1–10.
- [8] Chevalier S, Larpin JP. Formation of perovskite type phases during the high temperature oxidation of stainless steels coated with reactive element oxides. *Acta Mater* 2002;50(12):3105–14.
- [9] Quaddakers WJ, Greiner H, Hansel M, Pattanaik A, Khanna AS, Mallener W. Compatibility of perovskite contact layers between cathode and metallic interconnector plates of SOFCs. *Solid State Ionics* 1996;91(1–2):55–67.
- [10] Linderoth S. Controlled reactions between chromia and coating on alloy surface. *Surf Coat Technol* 1996;80(1–2):185–9.
- [11] Orlovskaya N, Coratolo A, Johnson C, Gemmen R. Structural characterization of LaCrO<sub>3</sub> perovskite coating deposited by magnetron sputtering on an iron based chromium containing alloy as a promising interconnect material for SOFCs. *J Am Ceram Soc.*
- [12] Azegami K, Yoshinaka M, Hirota K, Yamaguchi O. Formation and sintering of LaCrO<sub>3</sub> prepared by the hydrazine method. *Mater Res Bull* 1998;33(2):341–8.
- [13] Hayashi H, Watanabe M, Inaba H. Measurement of thermal expansion coefficient of LaCrO<sub>3</sub>. *Thermochim Acta* 2000;359(1):77–85.
- [14] Suda E, Pacaud B, Seguelong T, Takeda Y. Sintering characteristics and thermal expansion behavior of Li-doped lanthanum chromite perovskites depending upon preparation method and Sr doping. *Solid State Ionics* 2002;151(1–4):335–41.
- [15] Xing L, Eckert J, Loser W. Local ordering upon crystallization of bulk amorphous alloys. *Ann Chiem Sci Mater* 2002;27(5):69–75.
- [16] Tourir H, Dixmier J, Zellama K, Morhange J, Elkaim P. Bimodal crystal size distribution in annealed r.f. magnetron silicon films: a memory effect of the local order inhomogeneities in the initial amorphous state. *J Non-Cryst Solids* 1998;227–230:906–10.
- [17] Oxtoby DW. Crystallization: diversity suppresses growth. *Nature* 2001;413:694–5.
- [18] Orlovskaya N, Johnson C, Gemmen R. Unpublished results.
- [19] Hashimoto T, Tsuzuki N, Kishi A, Takagi K, Tsuda K, Tanaka M, Oikawa K, Kamiyama T, Yoshida K, Tagawa H, Dokiya M. *Solid State Ionics* 2000;132:183.
- [20] Furusaki A, Konno H, Furuichi R. Pyrolytic process of La(III)–Cr(VI) precursor for the perovskite type lanthanum chromium oxide. *Thermochim Acta* 1995;253:253–64.
- [21] Hoang DL, Dittmar A, Radnik J, Brzezinka K, Witke K. Redox behavior of La–Cr compounds formed in CrO<sub>x</sub>/La<sub>2</sub>O<sub>3</sub> mixed oxides and CrO<sub>x</sub>/La<sub>2</sub>O<sub>3</sub>/ZrO<sub>2</sub> catalysts. *Appl Catal A Gen* 2003;239:95–110.
- [22] Thorpe MF, Jacobs DJ, Chubynsky MV, Philips JC. Self-organization in network glasses. *J Non-Cryst Solids* 2000;266–269:859–66.
- [23] Wang Y, Nakaoka T, Murase K. Structural relaxation and self-organization in network glasses at stiffness transition. *J Non-Cryst Solids* 2002;307–310:772–7.
- [24] Araki H. Micro-area X-ray diffraction techniques. *Rigaku J* 1989;6(2):34–42.
- [25] Hoang DL, Dittmar A, Schneider M, Trunschke A, Lieske H, Brzezinka K, Witke K. Evidence of lanthanum–chromium mixed oxides formed in Cr<sub>x</sub>/La<sub>2</sub>O<sub>3</sub> model catalysts. *Thermochim Acta* 2003;400:153–63.